Available online at www.sciencedirect.com
SCIENCE DIRECT®
Journal of Catalysis 223 (2004) 86–97
JOURNAL OF CATALYSIS
www.elsevier.com/locate/jcat

HDS of dibenzothiophene over polyphosphates supported on mesoporous silica

B. Pawelec,[a] S. Damyanova,[b,*] R. Mariscal,[a] J.L.G. Fierro,[a] I. Sobrados,[c] J. Sanz,[c] and L. Petrov[b]

[a] *Instituto de Catalisis y Petroleoquimica, CSIC, C/ Marie Curie 2, Cantoblanco, 28049 Madrid, Spain*
[b] *Institute of Catalysis, Bulgarian Academy of Sciences, 1113 Sofia, Bulgaria*
[c] *Instituto de Ciencias de Materiales, CSIC, Cantoblanco, 28049 Madrid, Spain*

Received 24 September 2003; revised 1 December 2003; accepted 13 January 2004

Abstract

Molybdophosphoric (HPMo) and tungstophosphoric (HPW) acid catalysts, supported on hexagonal mesoporous silica (HMS) carriers and modified with Ti, Zr, and Zr + Al, were prepared. The catalysts were characterized by Fourier transform IR spectroscopy of adsorbed pyridine and deuterated acetonitrile, X-ray photoelectron spectroscopy, and ^{31}P and ^{1}H nuclear magnetic resonance. Catalytic activity was tested in the hydrodesulfurization reaction of DBT. The thermal stability and the properties of the supported molybdophosphates and tungstophosphates were discussed in terms of support effect. For the hydrodesulfurization reaction, which was carried out under high hydrogen pressure, the HPMo/ZrAlHMS catalyst had higher activity and selectivity to biphenyl formation than the other supported HPMo catalysts. Regardless of the carrier, supported HPW catalysts were the most active.

Keywords: Deep hydrodesulfurization; DBT; Mesoporous silica; Polyphosphates

1. Introduction

Heteropoly acid (HPA) compounds with a Keggin-type anion and their derivatives are industrial catalyst precursors and are used in many catalytic reactions [1–6]. However, there are few reports on the use of supported HPAs in the hydrodesulfurization (HDS) reaction. Most studies have focused on molybdenum HPA, which was used only in model studies to investigate the HDS of thiophene [7–9]. It has been shown [8] that supported 12-molybdophosphoric acid (HPMo) and its Co and Ni salts are good oxide precursors for thiophene HDS. Work in the field of deep HDS has become more intense in the last few years; a detailed general account of deep HDS, dealing with new catalysts, the effects of solvents and feedstock, kinetics and mechanisms, the effects of the support, and catalyst synergy has been reviewed by Vasudevan and Fierro [10].

Owing to the importance of heteropoly compounds for a variety of oxidation reactions, as well as for their application in hydrotreatment reactions, their structural stability as a function of temperature and reaction atmosphere and their structural transformation during catalyst activation are important aspects for understanding the working catalyst system. Different carriers have been used to support HPAs, and their thermal stability has been shown to depend on the type of the support and the loading of HPA. MCM-41 mesoporous systems are especially suitable for depositing large HPAs precursors. This mesoporous material has a hexagonal array of uniform pores (1–5 to 10 nm) and a very large surface area [11,12]. The unique properties of MCM-41 make them potentially useful for catalytic application in reactions such as deep HDS. This type of molecular sieve has been studied in depth as a support for deep HDS Mo catalysts promoted with Co or Ni [13–19]. No work on deep HDS on HPAs catalysts supported on mesoporous materials has been published. Kozhevnikov and co-workers [20] showed that HPW acid, supported on silica with a large surface area, is a good catalytic system for efficient HDS of dibenzothiophene (DBT) under conditions similar to those in industry.

In our previous work [21], we attempted to immobilize the 12-molybdophosphoric, $H_3PMo_{12}O_{40}$, and the 12-tungstophosphoric, $H_3PW_{12}O_{40}$ (HPW) heteropoly acids on hexagonal mesoporous silica (HMS) with a large surface

* Corresponding author.
E-mail address: soniad@satline.net (S. Damyanova).

0021-9517/$ – see front matter
doi:10.1016/j.jcat.2004.01.018

area modified with different cations. The textural and surface properties of HMS were modified by adding Ti, Zr, and Al cations. Small-angle diffraction peaks and the large surface area of metal-containing HMS samples demonstrated that these materials, prepared by means of a neutral template, have a mesoporous crystalline structure. Incorporation of Zr and Al cations led to the development of textural mesoporosity in addition to the framework mesoporosity [21], characteristic of HMS and Ti-containing mesoporous silica materials.

This work is one of the first attempts to demonstrate that supported heteropoly acids are good oxidic precursors for the active sulfided phase for HDS of DBT. In the present work we concentrated on (i) the effect of cations in metal-substituted HMS supports, (ii) the thermal stability of molybdo- and tungstophosphate anions, (iii) the properties of the catalyst surface, and (iv) the catalytic activity of MeHMS-supported HPMo and HPW acids in the HDS reaction of DBT. The DBT was selected for activity tests for the following reasons: (i) DBT is a chemically and thermally more stable S-containing molecule than thiophene. (ii) It is a large S-containing molecule, in which the steric hindrance of the two phenyl groups may inhibit accessibility to surface sites. (iii) Both HDS and hydrogenation functionalities can be examined simultaneously. The catalysts were characterized by Fourier transform IR spectroscopy (FTIR) of adsorbed pyridine and deuterated acetonitrile, ^{31}P and ^{1}H nuclear magnetic resonance (NMR), and X-ray photoelectron spectroscopy (XPS) techniques in an attempt to explain the relationship between the catalyst structure and the activity and selectivity of the catalysts.

2. Experimental

2.1. Preparation of the samples

Details about the preparation of metal-containing hexagonal mesoporous silica (MeHMS) carriers have been published [21]. Two series of supported heteropoly acids were prepared. The first was obtained by wet impregnation of HMS and metal-containing HMS carriers with an aqueous solution of 12-tungstophosphoric acid (Aldrich reagent grade) of the appropriate concentration at pH $\leqslant$ 3. The second series of catalysts corresponds to 12-molybdophosphoric acid (Aldrich reagent) supported on the mesoporous materials, prepared as described above. The resulting solids were dried and calcined in a flow of air at 343 and 623 K, respectively. The samples were designated HPW(HPMo)/MeHMS, where Me is Ti, Zr, and/or Zr + Al. The amount of W(Mo) in each sample was about 17 wt%.

2.2. Methods

Framework vibration spectra in the range of 4000 to 400 cm^{-1} were recorded on a Fourier transform infrared Nicolet 5 ZDX spectrophotometer at a resolution of 4 cm^{-1}. Each spectrum was averaged over 100 scans. Wafers were prepared by diluting a pellet of the sample (1:100) in KBr. IR spectra of chemisorbed pyridine and deuterated acetonitrile (CD_3CN) were recorded at room temperature. Self-supporting wafers (ca. 10 mg/cm^2) had been outgassed under vacuum at 473 K for 1 h in an infrared vacuum cell equipped with greaseless stopcocks and KBr windows. After introducing the pyridine and CD_3CN at room temperature (5 Torr in both cases), the fraction of physically adsorbed molecules was removed by outgassing at room temperature for 5 min in the case of CD_3CN and at 393 K for 1 h in the case of pyridine. The net infrared spectra of chemisorbed pyridine and CD_3CN were obtained after subtracting the background spectrum of the solid.

The X-ray photoelectron spectra of the calcined and used catalysts were recorded on a VG Escalab 200R electron spectrometer equipped with a hemispherical electron analyzer, using an Mg-K$_\alpha$ ($h\nu = 1253.6$ eV) X-ray source. The ECLIPSE software was used to record and analyze the spectra. The used samples, kept in *i*-octane to avoid exposure to air, were outgassed at 10^{-5} mbar and then transferred to the ion-pumped analysis chamber; the residual pressure was below 7×10^{-9} mbar during data acquisition. Mo $3d_{5/2}$, W $4f_{3/2}$, Ti $2p_{3/2}$, P 2p, Si 2p, and Al 2p core-level spectra were recorded. The binding energy (BE) of the Si 2p peak of the support at 103.4 eV was taken as the internal standard (accuracy within $\pm$0.1 eV). Each spectral region of the photoelectrons of interest was scanned a number of times to obtain a good signal-to-noise ratio. The intensity of the peaks was estimated by calculating the integral of each peak after subtracting an S-shaped background [22] and fitting the experimental peak to a combination of Lorentzian/Gaussian lines of variable proportions.

Solid-state MAS-NMR was performed on an MSL 400 Bruker spectrometer at room temperature. Frequencies of 161.96 (^{31}P signal) and 400.13 MHz (^{1}H signal) were used. Samples were spun at 10 to 12 kHz, and spectra were taken after $\pi/2$ pulse irradiation (6 and 4 µs, respectively). The time interval between successive scans was 2 to 20 s, depending on the spin-lattice relaxation times of the nuclei. The number of scans was 100 to 300. ^{1}H spectra were referenced to an external sample of trimethylsilane (TMS (0 ppm)), while ^{31}P NMR spectra were referenced to an 85% H_3PO_4 solution (0 ppm).

2.3. Test reaction

The catalysts were tested in the HDS reaction of DBT (1 wt% of DBT dissolved in *n*-decaline (Aldrich, 99% purity)). The reaction was carried out in a bench-scale, high-pressure down-flow reactor. To avoid hot spots, 0.25 g of catalyst was diluted with 0.5 g of SiC. After heating the catalyst at 473 K for 0.5 h in an N_2 flow (100 ml/min), the catalyst was activated in the stream of a mixture H_2 and H_2S (10:1) at a flow rate of 50 ml/min at 623 K for 2 h. Activa-

tion was followed by purging in a flow of N_2 at 573 K for 15 min. The system was pressurized with H_2 at $P = 30$ bar, and the liquid feed of 1 wt% DBT dissolved in *n*-decaline and H_2 was passed through the reactor. The reaction conditions for the Mo series were: 553–573–593 K, H_2 flow rate of 5800 ml (STP)/h, $P = 30$ bar, and weight hourly space velocity (WHSV) $= 35\ h^{-1}$. The samples containing W were treated under the same conditions, except that the temperatures were 553, then 563, and finally 573 K; the reaction lasted 1 h at each temperature. Since the sulfidation of tungsten oxide is more difficult than that of molybdenum oxide [23], the activation of the tungsten precursor was accomplished at a higher temperature than the activation of the Mo counterparts (723 vs 623 K).

Samples were collected periodically and analyzed by GC with an FID (Varian chromatograph Model Star 3400 CX) equipped with a DB-1 column (30 m × 0.53 mm, 100% methylpolysiloxane, J & W Scientific as the stationary phase). In addition to unreacted DBT, biphenyl (BP) and cyclohexylbenzene (CHB) were the only products detected. The total DBT conversion was calculated as the disappearance of DBT. Selectivity on BP and CHB are given by equations (1) and (2), respectively,

$$S_{BP} = \frac{x_{BP}}{x_{BP} + x_{CHB}} 100, \quad (1)$$

$$S_{CHB} = \frac{x_{CHB}}{x_{BP} + x_{CHB}} 100, \quad (2)$$

where x_i is the degree of conversion for *i*th components of the reaction mixture.

3. Results and discussion

3.1. XPS data

Analysis of the Mo $3d_{5/2}$, W $4f_{7/2}$, Si 2p, Ti $2p_{3/2}$, P 2p, and Al 2p core levels provided useful information about the chemical state of the elements and their relative proportions at the surface of the samples. Table 1 gives the binding energies of Mo $3d_{5/2}$, W $4f_{7/2}$ electrons for oxide and used catalysts. The distribution of the Mo(W) oxidation state is expressed as a percentage of the area. Fig. 1 shows the XPS spectra of the spent HPMo/MeHMS and Fig. 2 of the spent HPW/MeHMS catalysts. The BE of Ti $2p_{3/2}$ at 459.2 eV did not change in the oxide and spent catalysts, confirming that the oxidation state of titanium is constant (Ti(IV)). The value of the BE for Ti $2p_{3/2}$ was slightly higher than for pure TiO_2, which may be due to the change in the coordination number of the cation arising from the electron transfer between the cation and the supported molybdenum and tungsten species. The BE value of P 2p at 133.9 eV for the spent HPMo/TiHMS catalyst was higher than that of the freshly prepared TiO_2-supported HPMo, with a BE at 132.9 eV [24].

The BE of the W $4f_{7/2}$ core electron levels at 36.1 eV for the supported oxide HPW catalysts (Table 1) can be related

Table 1
S_{BET} and XPS parameters for oxide and spent mesoporous-supported HPMo and HPW catalysts

Sample	S_{BET} (m^2/g)	Oxidic catalysts BE (eV)		Spent catalysts BE (eV)	
		Mo $3d_{5/2}$	W $4f_{7/2}$	Mo $3d_{5/2}$	W $4f_{7/2}$
HPMo/HMS	751	233.3 (58)		232.8 (16)	
		231.8 (42)		229.7 (84)	
HPMo/TiHMS	532	233.1 (50)		232.9 (50)	
		231.8 (50)		229.7 (50)	
HPMo/ZrHMS	641	233.4 (46)		232.7 (54)	
		232.0 (54)		229.8 (46)	
HPMo/ZrAlHMS	531	233.2 (58)		232.7 (40)	
		231.8 (42)		229.7 (60)	
HPW/HMS	774		36.1 (65)		35.4 (27)
			34.7 (35)		32.4 (73)
HPW/TiHMS	595		36.1 (65)		35.5 (28)
			34.7 (35)		32.3 (72)

Peak percentages are in parentheses.

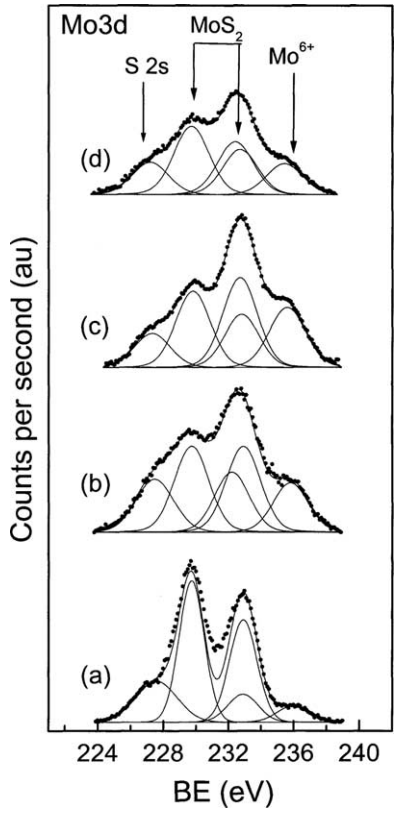

Fig. 1. XPS spectra of Mo 3d core levels for spent HPMo/HMS (a) and HPMo/MeHMS catalysts, modified with different cations: Ti (b), Zr (c), and Zr + Al (d).

to the W(VI) species [25]. A small percentage of the partially reduced W species is present in the oxide samples (BE of W $4f_{7/2}$ at 34.7 eV) (Table 1). The BE for Mo $3d_{5/2}$ at 233.1 and 231.8 eV for the supported HPMo samples corresponds to the presence of fully oxidized molybdenum (Mo(VI)) [26] and partially reduced molybdenum (Mo(V)) species [27], respectively, coordinated by O^{2-} and/or OH^- ions. The percentage of the latter species is almost the same as for HPMo

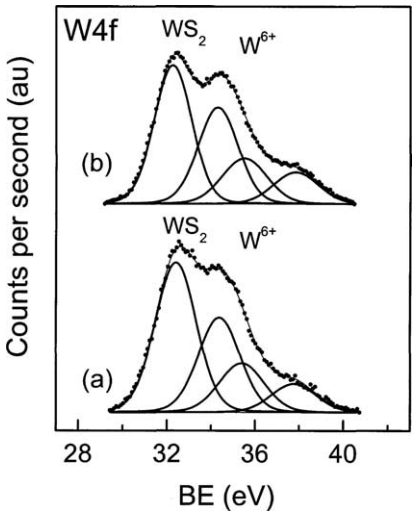

Fig. 2. XPS spectra of W 4f core levels for spent HPW/HMS (a) and HPW/TiHMS (b) catalysts.

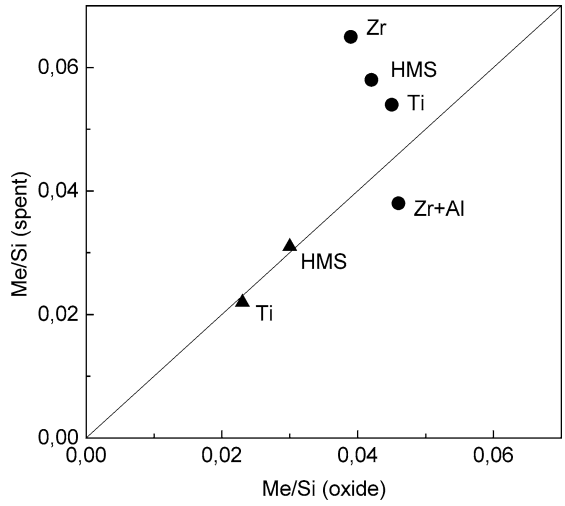

Fig. 3. XPS atomic Me/Si ratios for spent versus calcined mesoporous–supported catalysts. Circles and squares correspond to HPMo- and HPW-supported catalysts, respectively.

supported on HMS, modified with Ti and Zr. The presence of partially reduced Mo and W species in the oxide samples may be due to: (i) electron transfer between the supported Mo and W and the support modified by cations, which can occur during preparation due to a strong interaction and (ii) photoreduction of the oxide species when the sample is exposed to the X-ray source in the chamber of the spectrometer see [24,28].

With the exception of HPMo/HMS, the resolution of the XPS Mo 3d (W 4f) spectra was poor for all the spent catalysts (Figs. 1 and 2). This was due to the presence of different types of surface molybdenum or tungsten species. As result of the spectral fitting, species with BE of Mo $3d_{5/2}$ at 232.8 and 229.7 eV were identified in the spent HPMo catalysts; they are assigned to Mo(VI) in an oxide and/or oxy-sulfiding surrounding [29] and to Mo(IV) of MoS_2, respectively [30]. The formation of Mo oxysulfide species (like $MoO_2S_2^{2-}$) is caused by the presence of tetrahedral molybdate groups, which interact strongly with the support and which are difficult to reduce and sulfide. The peak on the side of the Mo 3d spectra (low binding energy) for the spent catalysts, characteristic of the 2s level of S^{2-} species ($\cong$ 226.2 eV) [31], was poorly resolved (S 2p spectra not reported here).

The percentages of the different molybdenum species, obtained from the Mo $3d_{5/2}$ core electron levels, are listed in parenthesis in Table 1. The following features are a consequence of the type of atom introduced into the HMS: (i) Total transformation of Mo oxysulfide species to MoS_2 was not achieved for all catalysts. The pretreatment and reaction conditions in this study were probably insufficient for reducing and sulfiding the tetrahedrally coordinated molybdenum species. (ii) The greatest amount of MoS_2 was observed for HPMo/HMS. (iii) The percentage of Mo oxysulfide species was $\geqslant$ 40% for HPMo supported on cation-modified HMS supports, indicating a strong interaction between the supported Mo species and the support.

The BE (35.4 eV) of spent, supported HPW catalysts suggests the presence of oxysulfide; the BE at 32.4 eV corresponds to WS_2-like species [32] (Table 1). Unlike supported HPMo catalysts, the relative percentage of oxysulfide and sulfided tungsten species did not change for the spent HPW/HMS and HPW/TiHMS catalysts (Table 1). In addition to the more difficult sulfidation of the W oxide species compared to the Mo oxide, due to differences in the polarization of the metal–oxygen bond [33], the percentage of sulfide W species in the HPW/TiHMS catalyst was significantly larger than that found for the HPMo/TiHMS catalyst.

The effect of the cation in the HMS support on the distribution of the supported active metals (Mo or W) was estimated from the XPS atomic intensity ratios (Mo(W)/Si) measured for the spent catalysts on different supports and plotted against the same ratio measured for the oxide samples (Fig. 3). From Fig. 3 it is clear that the dispersion of the Mo species was affected by the type of the modifying cation in the support. Introduction of Zr and Al into the HMS led to a greater dispersion of oxide molybdenum species on the surface of the support (Fig. 3). This is probably due to the disintegration of the large oxoanions into smaller structures, which remain well dispersed on the surface due to the stronger interaction between the anions and the modified support. However, with the exception of HPMo supported on ZrAl/HMS, all the spent HPMo catalysts had higher Mo/Si ratios, indicating a better dispersion of molybdenum sulfide species, especially in the case of the sample containing Zr. Supported HPW samples had the same ratios in the oxide and the spent catalysts with respect to the type of the support (Fig. 3); this indicates that the uniform state of the W species is the same before and after the reaction. The W/Si ratios are lower than the Mo/Si ratios, suggesting aggregation of anchored tungstophosphate anions and of sulfide W species on the surface of the supports.

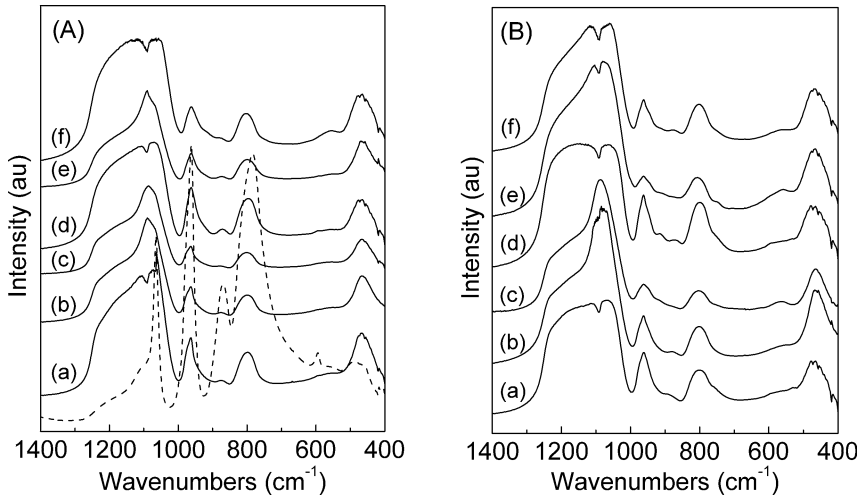

Fig. 4. IR spectra of HPMo/HMS (A, a–c), HPMo/TiHMS (A, d–f), HPMo/ZrHMS (B, a–c), and HPMo/ZrAlHMS (B, d–f) after different temperature treatments at 343 (a, d), 523 (b, e), and 623 K (c, f). Dashed line corresponds to bulk HPMo.

3.2. FTIR study

3.2.1. Integrity of the Keggin structure

The IR spectra of the samples heated at different temperatures reveal a change in the intensity and position of the characteristic IR bands of the Keggin anion structure in bulk HPMo and HPW as well as on the surface of supported HPMo and HPW. The IR spectra of the HPMo and HPW acids, supported on HMS and metal-substituted HMS carriers, and after exposure to different calcination temperatures are shown in Figs. 4 (HPMo) and 5 (HPW). The IR spectra of bulk HPMo and HPW are also presented in the corresponding figures. It is well known [34] that the Keggin structure of HPMo and HPW acids consists of one PO_4 tetrahedron surrounded by four trimetallic groups of three edge-sharing MO_6 (M = Mo or W) octahedra. The IR spectrum of bulk HPMo (Fig. 4) shows bands at 1065, 963, 873, and 787 cm^{-1}, assigned to the stretching vibrations ν_{as}(P–O_d), ν_{as}(Mo–O_t), ν_{as}(Mo–O_b–Mo), and ν_{as}(Mo–O_c–Mo), respectively, which characterize the Keggin unit [24]. The bands at 1080, 982, 891, and 793 (Fig. 2a) characterize the heteropoly anion vibrations in the HPW acid [34] (Fig. 5). The bands at 1080 and 982 cm^{-1} correspond to the stretching vibrations of P–O_d and W=O_t bonds, respectively, while the other two bands correspond to W–O_b–W vibrations.

Some of the bands of the supported HPAs (1200 to 400 cm^{-1}) were partially or fully covered by the bands of the supports (Figs. 4 and 5). Two strong bands appeared in the spectrum of HMS-supported HPMo at 966 and 800 cm^{-1} (Fig. 4A,a), caused by the overlapping of the IR absorption bands of silica close to 967 and 802 cm^{-1}, and those of the HPMo acid at 963 and 787 cm^{-1}. A band of very low intensity at about 876 cm^{-1} was also observed. The Keggin structure was preserved in the HMS-supported HPW sample, as revealed by the presence of bands at 983 and 896 cm^{-1} (Fig. 5a). The strong band at about 808 cm^{-1} may be due to the overlapping of the support band and the band assigned

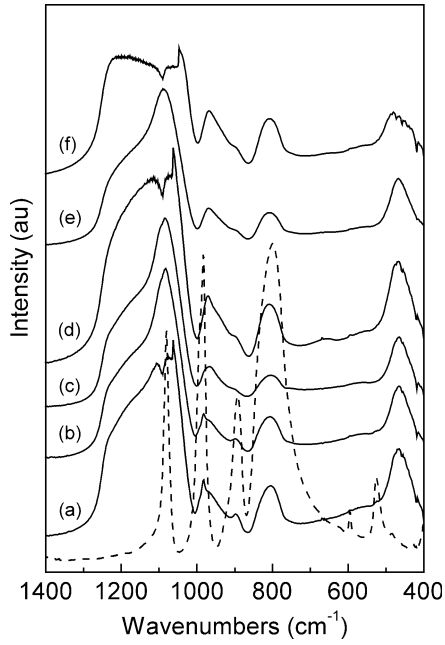

Fig. 5. IR spectra of HPW/HMS (a–c) and HPW/TiHMS (d–f) after different temperature treatments at 343 (a, d), 523 (b, e), and 623 K (c, f). Dashed line corresponds to bulk HPW.

to the bridging W–O_b–W bonds in the heteropolyanion. The bands, which characterize the (P–O_d) asymmetric vibrations at 1063 and 1080 cm^{-1} in all the supported HPMo and HPW samples, respectively, were strongly masked by the intense band of the HMS support at 1090 cm^{-1}. In the spectra of the HMS-supported HPMo this appeared as a shoulder at about 1060 cm^{-1} in the strong 1090 cm^{-1} carrier band. Consequently, the Keggin unit is mainly characterized by the stretching modes assigned to terminal Me–O and bridging Me–O_b–Me bonds.

All the bands of the phosphomolybdate and phosphotungstate heteropolyanions were present in the IR spectra of the supported samples and underwent a frequency shift

and/or broadening (Figs. 4 and 5). This is in agreement with the ^{31}P NMR results, which also show that the ^{31}P signal underwent a significant shift from that of the hydrated unsupported HPW and HPMo acids. It is assumed that the Keggin structure remained on the HMS support after impregnation with HPMo and HPW acids, as shown by the agreement between the IR bands of the bulk and the supported heteropoly acids (Figs. 4A,a and 5a). Introduction of Ti into the HMS support hardly influenced the structure of the supported HPMo; the bands were preserved (Fig. 4A,c). A more significant change in the position and broadening of the IR bands of HPMo was observed after introduction of Zr and Zr + Al cations into the silica; this was more pronounced in the second case (Fig. 4B): (i) The Mo–O_t band split into two bands at 960 and 945 cm^{-1}. (ii) New bands appeared at 912 and 749 cm^{-1}. (iii) The intensity of the 960 cm^{-1} band of the AlZrHMS-supported HPMo sample was higher than that of the ZrHMS-supported sample. This indicates strong distortion of the heteropolyanion and the presence of new species on the surface. The splitting of the band attributed to the Mo=O_t bond and the appearance of the band at 749 cm^{-1} is related to the presence of a lacunary-type heteropolyanion with a defective Keggin structure, for example, $PMo_{11}O_{39}^{7-}$ [35]. The strong band at 960 cm^{-1} indicates a strong interaction between the support and the molybdenum species and the formation of Si–O–Mo and/or Zr(Al)–O–Mo bonds, as reported elsewhere [6].

Incorporation of Ti into the HMS-supported HPW led to a shift in the bands related to ν_{as}(W–O_t) mode (to 972 cm^{-1}) and ν_{as}(W–O_b–W) (to 897 cm^{-1}), compared with those of bulk HPW (Fig. 5d). This was probably due to the interaction of the cation-modified support surface, which weakens the interaction between the bonds in the heteropolyanion, leading to a significant distortion and loss of heteropolyanion symmetry.

Upon heating of the supported HPW and HPMo acids, they behaved differently on mesoporous materials, depending on the cations introduced into the support (Figs. 4 and 5B). All the bands ascribed to the Keggin unit in the MeHMS-supported HPMo samples were still present at 623 K but with low intensity (Figs. 4A and 4B). When the temperature was increased to 523 K, the band at 983 cm^{-1}, due to the ν_{as} vibration of W=O_t, was present in the spectra of HMS-supported HPW acid (Fig. 5). However, above this temperature the band shifted to the region of lower energy compared with the observed for the fresh-prepared sample (Fig. 5b and c), indicating that the anion was less cohesive due to its interaction with the support. The bands at 896 and 808 cm^{-1}, arising from the vibrations of the bridging W–O_b–W bonds, became less intense. The same was observed for the TiHMS-supported HPMo and HPW up to 623 K.

There was no significant change in the position of the IR bands for the ZrHMS- and ZrAlHMS-supported HPMo samples with increasing temperature (up to 623 K) (Fig. 4B). However, the bands were less intense. When the temperature was increased to 523 K, the split band of the ν_{as}(Mo–O_t) mode shifted to 962 cm^{-1} for the ZrHMS- and ZrAlHMS-supported HPMo due to the interaction between the modified support and the supported molybdenum species, as indicated above. Trace bands corresponding to vibrations of the Keggin unit were still recognizable in the spectra of the sample pretreated at 623 K.

3.2.2. Nature of the acid sites

3.2.2.1. FTIR of adsorbed pyridine. The spectra recorded after the adsorption of pyridine at room temperature on mesoporous-supported HPMo and HPW acid catalysts, outgassed at 393 K, are shown in Figs. 6A and 6B, respectively. The spectra show bands at 1453 and 1543 cm^{-1}, attributed to coordinately bonded pyridine on Lewis acid sites and pyridinium ion on Brønsted acid sites, respectively. As shown in Fig. 6, the supported acids retained at least some of their characteristic Brønsted acidic properties. The number of Lewis acid sites in these samples should be proportional to the increase in the number of exposed atoms, since silica shows only weak Lewis acid-

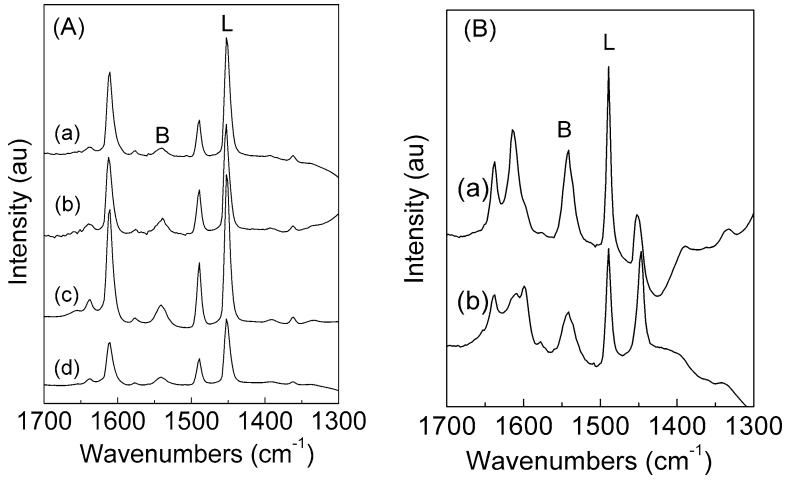

Fig. 6. IR spectra of adsorbed pyridine on HPMo (A) and HPW (B) catalysts supported on HMS (a), TiHMS (b), ZrHMS (c), and ZrAlHMS (d).

Table 2
Total DBT conversion, selectivity to BP formation obtained at 573 K, [CHB]/[BP] selectivities ratio, and activation energies (E_{act}) of mesoporous-supported HPMo and HPW catalysts

Samples	r (mmol/(h g_{cat}))	Conversion (%)	S_{BP}[a]	[CHB]/[BP][a]	E_{act} (kJ/mol)
HPMo/HMS	39	16.9	63.9	0.56	74.0
HPMo/TiHMS	41	17.8	56.4	0.77	80.5
HPMo/ZrHMS	39	17.7	75.6	0.32	117.8
HPMo/ZrAlHMS	61	25.8	77.7	0.29	100.9
HPW/HMS	62	26.7	81.0	0.24	150.5
HPW/TiHMS	110	47.2	97.4	0.03	145.3

[a] Calculated at the same DBT conversion (20%).

ity. Consequently, the high intensity of the band due to pyridine adsorbed on Lewis acid sites in the samples is result of the different Lewis acid sites capable of adsorbing pyridine: Mo^{6+}, Zr^{4+}, Ti^{4+}, and/or Al^{3+} cations. The surface Brønsted acid sites in the supported HPMo and HPW catalysts are associated with molybdenum (Mo^{6+}–OH) and tungsten species (W^{6+}–OH), respectively. The observed trend for the Lewis acid sites was Mo/ZrHMS > Mo/TiHMS > Mo/HMS = Mo/AlZrHMS, whereas the observed trend for the Brønsted acid sites was Mo/ZrHMS > Mo/HMS = Mo/TiHMS > Mo/AlZrHMS (Fig. 6A). It is assumed that the acidic component is the largest for the Zr-containing HPMo/HMS catalyst. Introduction of both metals (Zr and Al) into the HMS support led to a decrease in the acidity of the supported HPMo. This suggests a change in the HPMo structure, brought about by the dispersion and/or the stronger interaction with the support, as confirmed by the higher XPS atomic Mo/Si ratio.

The HPW catalysts supported on HMS and TiHMS showed higher Brønsted acidity (Fig. 6B) than the supported HPMo catalysts. The intensity of the bands representing Brønsted acidity was higher for the HPW/HMS sample, while the introduction of Ti into the HMS support caused a decrease in Brønsted acidity. This means that the acidic protons were retained in the acidic HPW phase on the surface of the mesoporous materials, as supported by the lower XPS atomic W/Si ratios as compared to those of the oxide-supported HPMo catalysts (Table 2).

3.2.2.2. FTIR of adsorbed deuterated acetonitrile. Information about the strength of Lewis acid sites was obtained from the position of the coordinatively bonded acetonitrile bands from 2300 to 2330 cm^{-1}, since the frequency usually increases with the acid strength of Lewis acid sites. Fig. 7 shows the net infrared spectra of CD_3CN adsorbed on HMS-supported HPMo samples. The use of the spectrum of pure mesoporous silica as a reference was published elsewhere [21]. The single C≡N stretching vibration band at 2274 cm^{-1} in the spectrum of HMS, the intensity of which decreased strongly for Mo/HMS and Mo/AlZrHMS, is associated with weakly bonded acetonitrile molecules

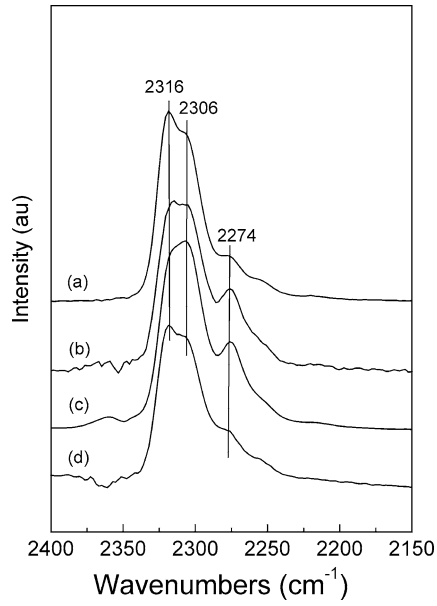

Fig. 7. IR spectra of CD_3CN adsorbed at room temperature on HPMo catalysts supported on HMS (a), TiHMS (b), ZrHMS (c), and ZrAlHMS (d).

on the hydroxyl groups, in agreement with the published data [36]. This assignment is consistent with the values for zeolite Y and ZSM-5 after CD_3CN sorption on Si–OH (2278 cm^{-1}) [37]. The observed trend in the intensity of the 2274 cm^{-1} band of the samples was Mo/ZrHMS = Mo/TiHMS ≫ Mo/HMS ≅ Mo/AlZrHMS. The lower intensity of the 2274 cm^{-1} band of the Mo/ZrAlHMS sample is related to the greater dispersion of the deposited molybdenum phosphate species due to a stronger interaction with the support surface. This is in agreement with the results of the XPS and FTIR measurements of adsorbed pyridine.

The band at 2306 cm^{-1} was assigned to the interaction of the CD_3CN molecule with Lewis acid sites, which can be bonded to coordinatively unsaturated tetrahedral Ti and Zr ions incorporated into the silica matrix [38] as well as to Mo. Considering the intensity of the 2306 cm^{-1} band, the trend in acidity was Mo/ZrHMS > Mo/HMS = Mo/TiHMS > Mo/AlZrHMS. The increase in the frequency of the IR band to 2316 cm^{-1} can be assigned to the presence of stronger Lewis acid sites, most probably due to the presence of highly unsaturated Mo atoms, which formed upon evacuation. The change in the intensity of the bands at 2306 and 2316 cm^{-1} was related to the steric hindrance of the deuterated acetonitrile, reducing the accessibility of the exposed atoms on the surface. The latter was correlated with the surface area of these samples (Table 1). The band indicative of the CD_3CN interaction with the strong Lewis sites at 2330 cm^{-1}, caused by nonframework aluminum, was not observed, as we showed for an AlZrHMS support [21]. This phenomenon was explained in terms of the covering of the support surface with molybdenum polyphosphate anions and/or the formation of an Al–O–Mo bond during the preparation of ZrAlHMS-supported HPMo.

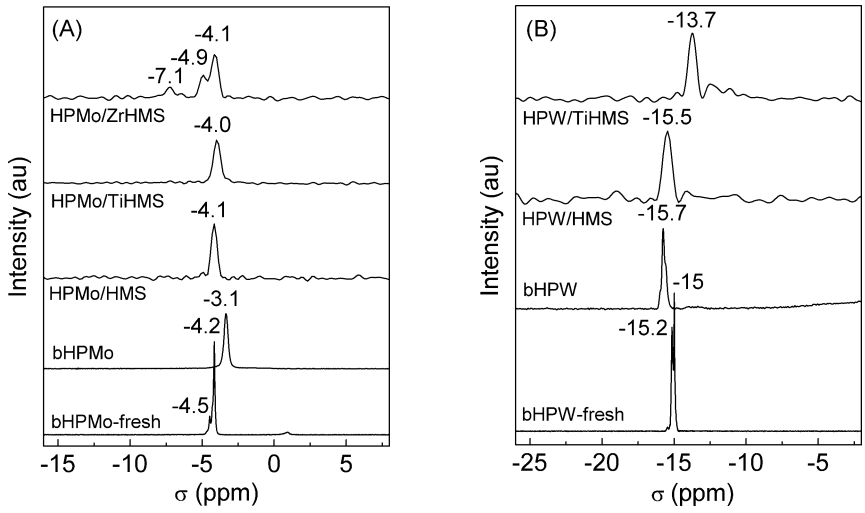

Fig. 8. ^{31}P NMR spectra of bulk and mesoporous-supported HPMo (A) and HPW (B) catalysts.

3.3. ^{31}P and ^{1}H NMR spectra

3.3.1. ^{31}P NMR spectra

Figs. 8A and 8B show the ^{31}P NMR spectra of mesoporous supported HPMo and HPW acid catalysts, respectively. Freshly unsupported HPMo exhibited an intense, sharp line with a chemical shift ($\sigma = -4.2$ ppm) (Fig. 8A), indicating a uniform phosphorus environment in the highly hydrated structure of HPMo acid [39]. The small peak close to the main peak at $\sigma = -4.5$ ppm is attributed to the fact that the hydration of the sample is not uniform. Similar to molybdophosphoric acid, the small difference in the chemical shift ($\sigma = -15.2$ and -15.0 ppm) of the ^{31}P NMR lines (Fig. 8B), characterizing $[PW_{12}O_{40}]^{3-}$ anions in fresh unsupported HPW acid [40], is due to the presence of heteropoly acid molecules with different numbers of crystallization water molecules. Increasing the temperature of calcination of bulk heteropoly acids up to 473 K led to the broadening of the ^{31}P NMR signals (Fig. 8), which corresponds to the formation of an anhydrous phase with a preserved Keggin unit due to the loss of crystallization water [41].

HPMo and HPW acids, supported on HMS, and metal-containing mesoporous materials revealed the broad line of the ^{31}P NMR (Fig. 8) compared to that of bulk acids (Fig. 8) after heating up to 473 K. This is attributed to the distortion of the heteropoly anion symmetry resulting from: (i) the interaction between the molybdophosphate or tungstophosphate anion and HMS or the metal-modified support and (ii) a loss of crystallization water molecules during the heating process. HPMo, supported on HMS and TiHMS, had ^{31}P NMR lines at $\sigma = -4.1$ ppm (Fig. 8A), characteristic of strongly dehydrated HPMo; the Keggin unit, however, was preserved, as was found in a previous study [21]. The ^{31}P NMR spectrum of HPMo supported on Zr-containing HMS showed that the ^{31}P lines had broadened and shifted considerably (Fig. 8A). The upfield shift of the resonance signal suggests that the heteropoly anion was destroyed; the new line at $\sigma = -7.1$ ppm is related to the stronger interaction of HPMo with the Zr cation, whereas the broad lines at $\sigma = -4.9$ and -4.1 ppm indicate the presence of dehydrated molybdophosphate anions. It is assumed that the interaction of supported HPMo with the carrier is rather weak on HMS and TiHMS and much stronger on ZrHMS. Although there are no spectra for the ZrAlHMS-supported HPMo, we suggest that this interaction must be much stronger on the surface of the ZrAlHMS support, due to the presence of Al in addition to Zr. It is well known [42,43] that alumina is unsuitable for supporting polyanions.

The ^{31}P NMR spectrum of HMS-supported HPW showed a broader and more intense band at $\sigma = -15.5$ ppm, similar to that of bulk HPW acid after heating at 473 K (Fig. 8B). According to Lefebre [44], the chemical shift of $\sigma = -15.7$ ppm is due to HPW which does not interact with the surface of the silica support. The downfield shift of the ^{31}P NMR resonance to -13.7 ppm for HPW supported on TiHMS is caused by the stronger interaction of the heteropoly anions with the surface of metal-modified silica; species of the type $(Me–O)^{n-}[H_{3-n}W_{12}PO_{40}]^{n-3}$ form as a result of the partial compensation in the charge of polyoxoanions by positively charged Ti cations. Furthermore, formation of lacunary-type heteropoly anion, such as $[PW_{11}O_{39}]$ Keggin units, cannot be ruled out.

3.3.2. ^{1}H NMR spectra

Figs. 9A and 9B show the ^{1}H NMR spectra of unsupported and mesoporous-supported HPMo and HPW acids, respectively. The spectra of bulk HPMo and HPW show two strong and sharp peaks with almost the same chemical shifts at $\sigma = 6.4$ and 7.3 ppm and at $\sigma = 6.8$ and 7.6 ppm respectively, suggesting that the protons have two different environments, depending on the degree of hydration. The peaks disappeared after heating to 473 K; broader, symmetric signals were observed at $\sigma = 8.0$ ppm for unsupported HPMo and at $\sigma = 5.0$ ppm for HPW acids. The ^{1}H NMR signal remained the same for all the supported samples after

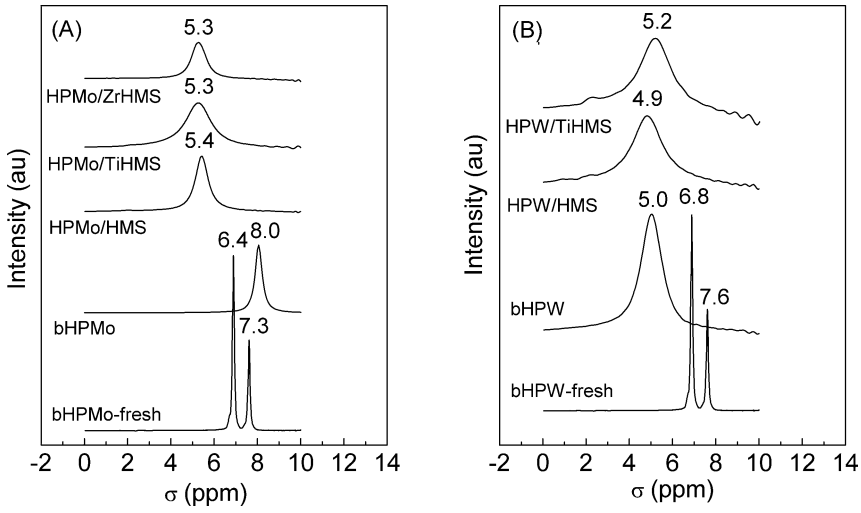

Fig. 9. ^{1}H NMR spectra of bulk and mesoporous-supported HPMo (A) and HPW (B) catalysts.

calcination at 473 K. The ^{1}H NMR signal was substantially broader for HPMo acid supported on Ti- and Zr-containing HMS compared to that of HPMo on HMS only (Fig. 9A). This was probably due to the stronger interaction of the protons with the metal-containing support. HPW acid supported on HMS and TiHMS showed ^{1}H NMR spectra that were about as broad ($\sigma = 4.9$ and 5.2 ppm, respectively) as for the fixed protons after the dehydration of polyanions.

3.4. Evaluation of catalysts in HDS of DBT

Table 2 lists the results of the catalytic tests at 573 K, giving the intrinsic activity, r, and the steady-state DBT conversion. DBT conversion occurred as follows: HPW/TiHMS $\gg$ HPW/HMS $>$ HPMo/ZrAlHMS $\gg$ HPMo/ZrHMS $\cong$ HPMo/TiHMS $>$ HPMo/HMS. Irrespective of the carrier, the samples prepared with tungsten precursors were more active than those prepared with Mo precursors. The Ti modification of the HMS carrier led to an increase in the catalytic activity of the HPW/HMS catalyst, while the introduction of Zr and Zr + Al to the HPMo/HMS samples had a stronger effect on BP formation and total DBT conversion, respectively.

As expected, the increase in the reaction temperature led to an increase in the catalytic activity of all the samples. Fig. 10 presents the Arrhenius plots of the temperature dependence of the rate constants. Table 2 gives the activation energies, derived from the Arrhenius plots. Regardless of the carrier, the HPW catalysts had higher apparent activation energies than the HPMo-containing catalysts. For the Zr- and ZrAlHMS-supported HPMo catalysts, the Arrhenius slopes were roughly parallel, indicating approximately the same activation energy for DBT conversion (Table 2).

Considering the temperature at which the catalysts reached 20% DBT conversion (Fig. 11), the lowest temperature of the HPW/TiHMS sample showed that it was the most active catalyst. Fig. 12 shows the temperature dependence of BP formation during the HDS of DBT. As expected, the

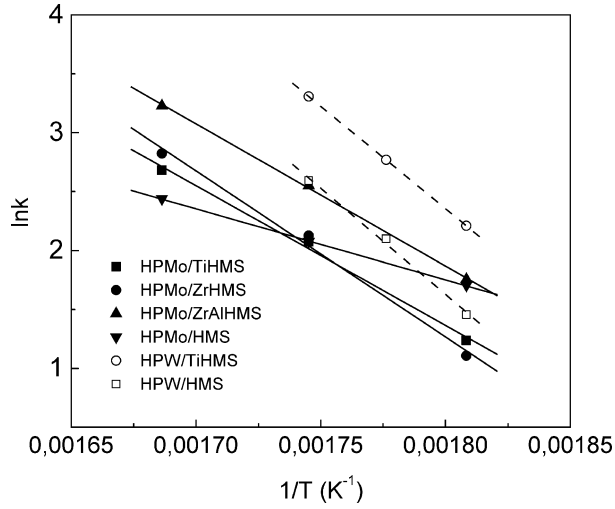

Fig. 10. Arrhenius plots of HDS of DBT over mesoporous-supported HPMo and HPW catalysts.

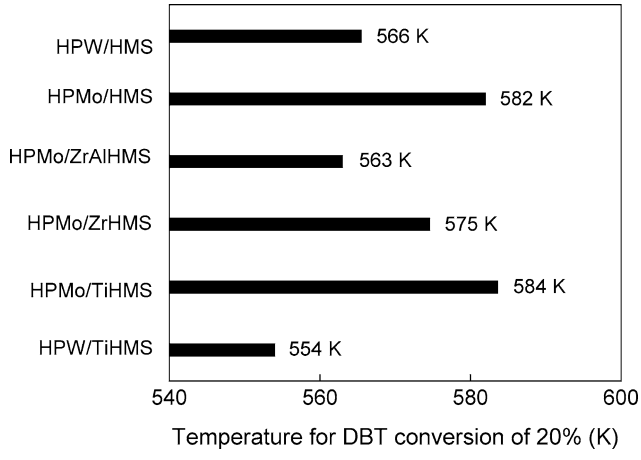

Fig. 11. DBT conversion of 20% as a function of reaction temperature for mesoporous-supported HPMo and HPW catalysts.

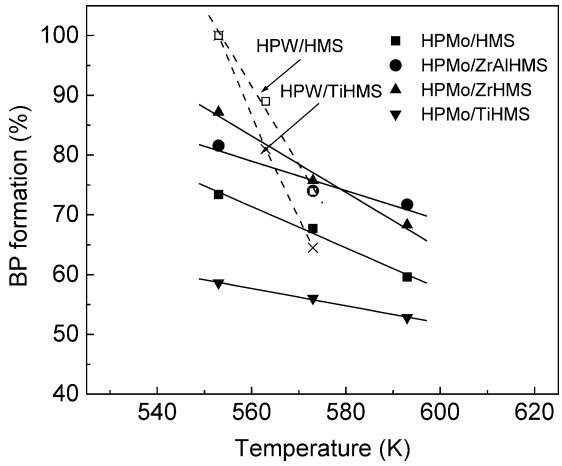

Fig. 12. Selectivity toward BP formation (%) as a function of the reaction temperature for mesoporous-supported HPMo and HPW catalysts.

increase in temperature led to a decrease in the BP formation of all the samples due to the higher selectivity toward CHB products. Of the supported HPMo catalysts, the higher BP selectivity of 20% DBT conversion for HPMo/ZrHMS and HPMo/ZrAlHMS (Table 2) indicates that these catalysts have lower hydrogenation activity than the HPMo/HMS and HPMo/TiHMS samples.

The activity data show the following: (i) The activation energy changes with the composition of the support and the metal precursor used (HPMo/HPW). (ii) The most reactive catalyst is HPW/TiHMS. (iii) All the catalysts have higher selectivity to biphenyl (calculated at 20% DBT conversion) than to cyclohexylbenzene formation. (iv) The selectivity to BP of HPMo/ZrHMS and HPMo/ZrAlHMS are almost the same, 75.6 and 77.7%, respectively. Although no intermediate hydrogenated products such as tetrahydrodibenzothiophene (TH-DBT) were observed, they may nevertheless have been present; they are often undetectable, because their desulfurization rate is extremely fast [45]. The reaction scheme is proposed to occur by two reaction routes in Refs. [46–48]:

$$\begin{array}{ccc} \text{DBT} & \rightarrow & \text{BP} \\ \downarrow & & \downarrow \\ \text{TH-DBT} & \rightarrow & \text{CHB}. \end{array} \qquad (3)$$

Based on this proposal we assume that the reaction mechanism in our study proceeds through a “parallel reaction mechanism,” in which CHB formation does not rely on the sequential hydrogenation product of BP. Therefore, BP may be classified as a product of C–S bond hydrogenolysis, whereas CHB is probably derived from DBT hydrogenation followed by desulfurization. According to the rim-edge model proposed by Daage and Chianelli [49] for unsupported MoS_2 catalysts, the active sites for BP and CHB formation may be the rim and edge plus rim sites, respectively. This is because of the steric hindrance of the adsorption of the DBT molecule on the edge sites, induced by its large size. Since the selectivity to HYD is related to the ratio of rim to edge sites of $MoS_2(WS_2)$, Table 2 lists [CHB]/[BP] selectivity ratios calculated at 20% of DBT conversion. From this table, the [CHB]/[BP] ratio of all the catalysts suggests low stacking of the $MoS_2(WS_2)$ particles and that this stacking increases with increasing temperature. In other words, the $MoS_2(WS_2)$ phase has a smaller number of edge sites compared to the rim sites. Furthermore, the most active HPW/TiHMS catalyst has the lowest [CHB]/[BP] ratio. Considering the rim-edge model of Daage and Chianelli [49], this suggests that the high activity of those catalysts is linked with the largest number of the rim sites formed on the WS_2 particles.

It is well known that the formation of well-dispersed Mo species on the support surface is essential for the preparation of high-performance HDS catalysts. Surface properties such as acidity affect the dispersion and the local environment of the metal species. The results show that the samples are very acidic, which strongly influences the conversion and product selectivity to HDS of DBT over sulfided samples. This supports the hypothesis that acidity enhances HDS and that different sites are involved in HDS and hydrogenation reactions. However, there is no direct correlation between the acidity and the reactivity of the catalysts. Compared to the Brønsted acidity of the fresh samples, the HPMo catalysts, supported on ZrHMS and ZrAlHMS carriers, exhibited the highest DBT conversion and the highest BP selectivity (Table 2), despite the difference in the Brønsted acidity. HPMo/ZrAlHMS had the lowest Brønsted acidity (Fig. 6A). Furthermore, the temperature, at which the HPMo/ZrAlHMS sample reached 20% DBT conversion (Fig. 11) was lower, showing that this catalyst was the most reactive catalyst of all the supported HPMo catalysts. This suggests that the presence of Brønsted acid sites is one of the necessary conditions for the HDS of DBT; this finding is similar to the conclusions reached for the HDS of thiophene [50].

The difference in the catalytic behavior does not seem to be related to the surface area of the catalysts. The intrinsic activity, related to the surface area of HPMo supported on ZrAlHMS, was the highest (Fig. 13); nevertheless its total surface area was the lowest (Table 1). Since all the HPMo and HPW samples, supported on metal-containing mesoporous carriers, do not contain any XRD patterns, the oxide molybdenum species were well dispersed on the surface, even at a relatively high Mo(W) loading. The best dispersion was observed for HPMo supported on ZrAlHMS, as confirmed by the lower intensity of the 2274 cm^{-1} band of the OH groups (Fig. 7) as well as by the higher XPS atomic Mo/Si ratio (Fig. 3).

It is, therefore, concluded that the stronger interaction between the electronegative molybdophosphate anions and the electropositive Zr and Al cations leads to the considerable distortion of the heteropoly anion, even during the impregnation process, and consequently to its destruction and to a better dispersion of oxide molybdenum species.

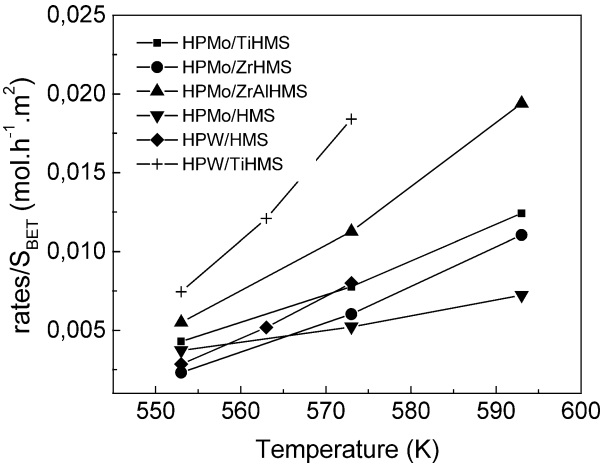

Fig. 13. Temperature dependence of the rates of S_{BET}.

However, the Mo/Si ratio of the spent HPMo/ZrAlHMS catalyst decreased significantly, indicating an agglomeration of the molybdenum sulfide phase. The Mo species of the spent HPMo catalysts, supported on HMS, Zr-, and Ti-containing HMS, showed better dispersion. However, for the latter two catalysts this dispersion is not linked to the dispersion of the molybdenum sulfide phase (MoS_2), because the percentage of Mo at a higher oxidation state is high in these catalysts (Table 1). This may be due to the fact that during sulfidation, the sulfur is incorporated into the bulk of the HPA and splits the molybdophosphate anions into smaller anions. This leads to the better dispersion of the molybdenum species and the formation of oxysulfide species.

The high proportion of oxysulfide molybdenum species in the HPMo catalysts supported on Zr- and Ti-containing HMS (Table 1) led to a lower specific activity per gram of catalyst (Table 2). It is assumed that the MoO_yS_x species, which formed at the support interface, probably act as a support for the MoS_2 phase, thus stabilizing the very small MoS_2 particles. This stabilization may be more difficult to achieve in the HPMo/HMS sample without the cation, despite the higher XPS Mo/Si ratio (Fig. 3). Moreover, hydrogenolysis is suppressed by the presence of H_2S and sulfur adsorbed on the molybdenum phase, whereas the hydrogenation of DBT is promoted by H_2S [51]. Therefore, the greater H_2S adsorption should increase on MoS_2 stabilized by MoO_xS_y species. It is assumed that H_2S adsorption on the agglomerated MoS_2 phase is lower for the HPMo/ZrAlHMS catalyst, considering the lower proportion of oxysulfide molybdenum species, which leads to lower hydrogenation selectivity (Table 2).

Introduction of Ti into the HMS carrier during the HDS of DBT causes a change in the product distributions for both the supported polyphosphate catalysts. Table 2 shows that the main increase in activity is related to the substantial increase in CHB formation, while BP formation was significantly retarded. The lower hydrogenation selectivity of the HPW/TiHMS catalyst compared to the unmodified HPW/HMS catalyst is related to a strong decrease in the Brønsted acidic character, as revealed by the IR spectra of adsorbed pyridine (Fig. 6B). In view of the above-noted mechanism, the number of active sites for hydrogenation increases and is favored by the greater H_2S adsorption on the dispersed WS_2 species (> 70%) (Table 1).

It is assumed that supported polyphosphates of Mo and W on mesoporous carriers are good oxide precursors for the active sulfided phase of the catalysts for the HDS of DBT. The change in the total DBT conversion and selectivity to BP and CHB formation of the catalysts is strongly influenced by the cation introduced into the HMS carrier; this cation leads to a change in the structure and surface properties of the supported catalyst.

Acknowledgments

Financial support of the project by the National Council of Scientific Research (CSIC) (Spain), and the Institute of Catalysis at the Bulgarian Academy of Sciences is gratefully acknowledged. B.P. acknowledges financial support from the Spanish Ministry of Science and Technology (Ramón and Cajal Project).

References

[1] S. Gao, J.B. Moffat, Catal. Lett. 42 (1996) 105.
[2] L.C. Passoni, A.T. Cruz, R. Buffon, U. Schuchadt, J. Mol. Catal. A 120 (1997) 117.
[3] I.V. Kozhevnikov, Chem. Rev. 98 (1998) 171.
[4] M. Mizuno, M. Misono, Chem. Rev. 98 (1998) 199.
[5] M.L. Cubeiro, S. Damyanova, J.L.G. Fierro, Catal. Lett. 49 (1997) 223.
[6] S. Damyanova, L.M. Gomez, M.A. Baňares, J.L.G. Fierro, Chem. Mater. 12 (2000) 501.
[7] A. Spojakina, S. Damyanova, D. Shopov, T.Kh. Shokhireva, T.M. Yurieva, React. Kinet. Catal. Lett. 27 (1985) 333.
[8] S. Damyanova, J.L.G. Fierro, Appl. Catal. A 144 (1996) 59.
[9] A. Griboval, P. Blanchard, E. Payen, M. Fournier, J.L. Dubois, Chem. Lett. 12 (1997) 1259.
[10] P.T. Vasudevan, J.L.G. Fierro, Catal. Rev.-Sci. Eng. 38 (1996) 161.
[11] J.S. Beck, J.C. Vartuli, W.J. Roth, M.E. Leonowicz, C.T. Kresge, K.D. Schmitt, C.T.W. Chu, D.H. Olson, E.W. Sheppard, S.B. McCullen, J.B. Higgins, J.C. Schlenker, J. Am. Chem. Soc. 114 (1992) 10834.
[12] C.T. Kresge, M.E. Leonowicz, W.J. Roth, J.C. Vartuli, J.S. Beck, Nature 359 (1992) 710.
[13] A. Wang, Y. Wang, T. Kabe, Y. Chen, A. Ishihara, W. Qian, J. Catal. 199 (2001) 19.
[14] C. Song, K.M. Reddy, Appl. Catal. A 176 (1999) 1.
[15] A. Wang, Y. Wang, Y. Chen, X. Li, P. Yao, T. Kabe, Stud. Surf. Sci. Catal. 142 (2002) 795.
[16] A. Wang, Y. Wang, T. Kabe, Y. Chen, A. Ishihara, W. Qian, P. Yao, J. Catal. 210 (2002) 319.
[17] X. Li, A. Wang, Y. Wang, Y. Chen, Y. Liu, Y. Hu, Catal. Lett. 84 (2002) 107.
[18] T. Klimova, M. Calderón, J. Ramírez, Appl. Catal. A 240 (2003) 29.
[19] X. Carrier, M. Che, Appl. Catal. A 253 (2003) 317.
[20] R. Shafi, M. Rafiq, H. Siddiqui, G.J. Hutchings, E.G. Derouane, I.V. Kozhevnikov, Appl. Catal. A 204 (2000) 251.
[21] S. Damyanova, L. Dimitrov, R. Mariscal, J.L.G. Fierro, L. Petrov, I. Sobrados, Appl. Catal. A, in press.
[22] D.A. Shirley, Phys. Rev. B 5 (1972) 4709.

[23] H. Topsøe, B.S. Clausen, F.E. Massoth, in: J.R. Anderson, M. Boudart (Eds.), Hydrotreating Catalysis, Science and Technology, vol. 11, Springer, Berlin, 1996.
[24] S. Damyanova, J.L.G. Fierro, Chem. Mater. 10 (1998) 877.
[25] D. Briggs, M.P. Seah, Practical Surface Analysis by Auger and X-Ray Photoelectron Spectroscopy, Wiley, Chichester, 1983, p. 620.
[26] S. Kasztelan, E. Payen, J.B. Moffat, J. Catal. 128 (1991) 479.
[27] J.G. Choi, L.T. Thompson, Appl. Surf. Sci. 93 (1996) 143.
[28] S. Damyanova, L. Petrov, P. Grange, Appl. Catal. A 239 (2003) 241.
[29] Th. Weber, J.C. Muijsers, J.H.M.C. van Wolput, C.P.J. Verhagen, J.W. Niemantsverdriet, J. Phys. Chem. 100 (1996) 14144.
[30] S. Damyanova, L. Petrov, M.A. Centeno, P. Grange, Appl. Catal. A 224 (2002) 271.
[31] A. Arteaga, J.L.G. Fierro, F. Delannay, B. Delmon, Appl. Catal. 26 (1986) 227.
[32] L. Salvati, L.E. Makovsky, J.M. Stencel, F.R. Brown, D.M. Hercules, J. Phys. Chem. 85 (1981) 3700.
[33] J.P. Mangnus, B. Scheffer, J.A. Moulijn, Am. Chem. Soc. Petrol. Div. Prepr. 32 (1987) 329.
[34] R. Thouvenot, M. Fournier, R. Franck, C. Rocchiccioli-Deltcheff, Inorg. Chem. 23 (1984) 598.
[35] P. Dufresne, E. Payen, J. Grimblot, J.P. Bonnele, J. Phys. Chem. 85 (1981) 2344.
[36] J.M. Chen, G. Thomas, G. Sankar, J. Chem. Soc., Faraday Trans. 90 (22) (1994) 3455.
[37] P.O. Scockert, F.D. Declerck, R.E. Sempels, P.G. Rouxhet, J. Chem. Soc., Faraday Trans. I 73 (1977) 359.
[38] R. Mariscal, M. Lopez-Granados, J.L.G. Fierro, J.L. Sotelo, C. Martos, R. Van Grieken, Langmuir 16 (2000) 9460.
[39] R. Thouvenot, C. Rocchiccioli-Deltcheff, M. Fournier, J. Chem. Soc., Chem. Commun. (1991) 1352.
[40] R. Massart, R. Contant, J. Fruchart, J. Cisbrini, M. Fournier, Inorg. Chem. 16 (1977) 2916.
[41] S. Damyanova, J.L.G. Fierro, I. Sobrados, J. Sanz, Langmuir 15 (1998) 469.
[42] K.M. Rao, R. Gobetto, A. Iannibello, A. Zecchina, J. Catal. 119 (1989) 512.
[43] W.C. Cheng, P. Luthra, J. Catal. 109 (1988) 163.
[44] F. Lefebre, J. Chem. Soc., Chem. Commun. (1992) 756.
[45] H. Farag, D.D. Whitehurst, K. Sakanishi, I. Mochida, Catal. Today 50 (1999) 49.
[46] A. Wang, Y. Wang, T. Kabe, Y. Chen, A. Ishihara, W. Qian, J. Catal. 199 (2001) 19.
[47] G.H. Singhal, R.L. Espino, J.E. Sobel, G.A. Huff, J. Catal. 67 (1981) 457.
[48] R. Shafi, G.J. Hutchings, Catal. Today 59 (2000) 423.
[49] M. Daage, R.R. Chianelli, J. Catal. 149 (1994) 414.
[50] J. Valyon, R.L. Schneider, W.K. Hall, J. Catal. 85 (1984) 277.
[51] B. Pawelec, R. Navarro, J.L.G. Fierro, P.T. Vasudevan, Appl. Catal. A 168 (1998) 205.